

Surface approximation from rapidly varying data: Applications to geophysical surfaces and seafloor surfaces

¹Apprato Dominique, ²Gout Christian and ³Le Guyader Carole

¹*Université de Pau et des Pays de l'Adour,*

²*Université de Valenciennes et du Hainaut Cambrésis,*

³*INSA de Rouen,*

France

1. Introduction

We propose an approximation method for surfaces with fault and /or large variations. We use image segmentation tools, meshing constraints, finite element methods and spline theory.

Curve and surface fitting using spline functions from rapidly varying data is a difficult problem (see Salkauskas, 1974, or Franke and Nielson, 1984, or Franke, 1982). In the bivariate case and without information about the location of large variations, usual approximation methods lead to instability phenomena or undesirable oscillations that can locally and even globally hinder the approximation (Gibbs phenomenon).

So, we propose a new method which uses scale transformations (see Apprato and Gout, 2000). The originality of the method consists of a pre-processing and a post-processing of the data. Instead of trying to find directly an approximant, we first apply a scale transformation to the z-values of the function. In the particular case of the approximation of surfaces, the originality of the method consists in removing the variations of the unknown function using a scale transformation in the pre-processing. And so the pre-processed data do not exhibit large variations. So we can use a usual approximant which will not create oscillations.

In case of vertical fault, we also propose an algorithm in order to find the location of large variations : the right approach to get a good approximant consists, in effect, in applying first a segmentation process to precisely define the locations of large variations and faults, and exploiting then a discrete approximation technique. To perform the segmentation step, we propose a quasi-automatic algorithm that uses a level set method to obtain from the given (gridded or scattered) Lagrange data, several patches delimited by large gradients (or faults). Then, with the knowledge of the location of the discontinuities of the surface, we generate a triangular mesh (which takes into account the identified set of discontinuities) on which a D^m -spline approximant (see Manzanilla 1986, Apprato et al., 1987, or Arcangéli et., 1997, or Arcangéli et al. 2004) is constructed.

We apply our method to different datasets (bathymetry, Lagrange data...): Piton de la Fournaise volcano in La Réunion island (see Gout and Komatitsch, 2000), Pyrenées

mountains in France (see Apprato et al., 2000), Marianas trench in the Pacific (see Apprato et al. 2002). We also give an example around the Hawaiian hot spot. The topography and bathymetry of the Hawaiian Islands in the Pacific ocean result from the activity of a huge hot spot combined with the effect of erosion. This hot spot has been more or less active since the Late Cretaceous, and as a result, the Big Island continues to grow, and to the East a new island is being formed.

2. Mathematical Modelling for surface approximation from Lagrange dataset

Unfortunately, when applied to the approximation of surfaces from rapidly varying data, usual methods like splines lead to strong oscillations near steep gradients, as illustrated in Figure 1. When the location of the large variations in the dataset is known, Salkauskas (1974) has proposed methods that use a spline under tension with a nonconstant smoothing parameter, and Hsieh and Chang (1994) have proposed a concept of virtual nodes inserted at the level of the large variations in the case of an approximant in the context of computer-aided geometric design. In the more general context where the location of the large variations in the dataset is not known *a priori*, Franke (1982) and Bouhamidi and Le Méhauté (1999) have proposed splines under tension belonging to more general spaces. These methods give good results in the case of curve fitting, but less accurate results in the case of surface fitting.

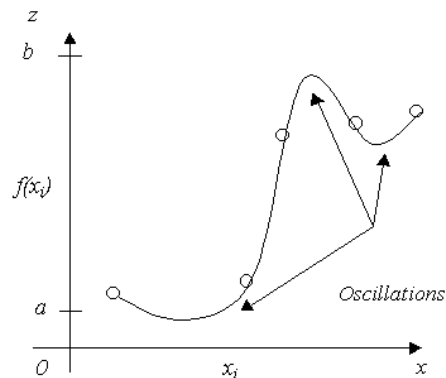


Fig. 1. When classical splines (for instance, here a C^1 spline) are used to interpolate data points $(x_i ; f(x_i))$ with large local variations, strong spurious oscillations are generated near steep gradients.

The new method we introduce here uses scale transformations, and is applied without any particular *a priori* knowledge on the data. The philosophy of the method is similar to interpolation methods based upon anamorphosed data commonly used in geostatistics (see, for instance, Issaks and Srivastava, 1989). In the first part of this article, a construction of the scale transformation families is presented. Results concerning the convergence of the approximation are given. We also show the efficiency of this innovative approach by applying it to the topography of the summit of the Piton de la Fournaise volcano, located in the Réunion Island (Indian Ocean, France). This volcano exhibits large and rapid variations

in steep river valleys in its southwestern part, as well as in a caldera, where the behavior of the method is tested.

The method we propose uses two scale transformations—namely φ_d for the preprocessing and ψ_d for the postprocessing. The first one, φ_d , is used to transform the z values representing the height of the unknown surface f into values (u_i) , regularly distributed in an interval chosen by the user, as illustrated in Figures 2A and 2B. The preprocessing function φ_d is such that the transformed data do not exhibit large local variations, and therefore a usual spline operator T_d can subsequently be applied without generating significant oscillations, as shown in Figure 2C. The second scale transformation ψ_d is then applied to the approximated values to map them back and obtain the approximated values of z (Figure 2D). It is important to underline that the proposed scale transformations do not create spurious oscillations. Moreover, this method is applied without any particular knowledge on the location of the large variations in the dataset. Let us consider a dataset

$(x_i^d, z_i^d)_{i=1, \dots, N(d)}^d$ indexed with a real d , such that when d tends to 0, the number of data points $N(d)$ tends to infinity. For the purpose of a theoretical study of the approximation convergence, we introduce a function $f: \Omega \rightarrow [a, b]$, such that the data set becomes $(x_i^d, z_i^d = f(x_i^d))_{i=1, \dots, N(d)}^d$.

The functions introduced above have the following expressions, for $m \in \mathbb{N}$:

$$- \varphi_d : [a, b] \rightarrow [\alpha, \beta] \subset \mathbb{R},$$

$$- T^d : (\varphi_d \circ f) \in H^m(\Omega, [\alpha, \beta]) \rightarrow T^d(\varphi_d \circ f) \in H^m(\Omega, [\alpha, \beta]), \quad (1)$$

$$- \psi_d \circ T^d(\varphi_d \circ f) \in H^m(\Omega, [a, b]),$$

where the preprocessing φ_d and the postprocessing ψ_d are continuous scale transformation families, where T^d is an approximation operator, for instance a spline, and where $H^m(\Omega, \cdot)$ denotes the usual Sobolev space. More precisely, we introduce a nonempty bounded connected set Ω of \mathbb{R}^2 with Lipschitz boundary, and an unknown function $f \in H^{m'}(\Omega, [a, b])$ that we want to approximate, this hypothesis allowing to have $(\varphi_d \circ f)$ bounded in $C^m(\overline{\Omega})$ (with $m' > m + 1$) a property used to establish the convergence of the approximation (Apprato and Gout, 2000). We also consider a subset A^d of $N = N(d)$ distinct points of $\overline{\Omega}$ such that

$$\sup_{x \in \Omega} \delta(x, A^d) = d \quad (2)$$

where δ is the Euclidean distance in \mathbb{R}^2 ; the index d represents the radius of the biggest sphere included in Ω that does not intersect with any point of A^d , and thus, when d tends to 0, the number of data points tends to infinity. We also introduce the set Z_1^d of $N = N(d)$ real numbers such that

$$\forall x_i^d \in A^d, f(x_i^d) \in Z_1^d \tag{3}$$

and the sequence Z_2^d of $p(d)$ distinct z values obtained from the ordering of Z_1^d ,

$$\forall \tilde{z}_i^d \in Z_2^d, i = 1, \dots, p(d),$$

$$a = \tilde{z}_1^d < \tilde{z}_2^d < \tilde{z}_3^d < \dots < \tilde{z}_{p(d)-1}^d < \tilde{z}_{p(d)}^d = b \tag{4}$$

where $[a, b] = \text{Im}(f)$. The sequence Z_2^d will be used for the construction of the scale transformation families in the following section. In what follows, for convenience, we also write z_i^d instead of \tilde{z}_i^d .

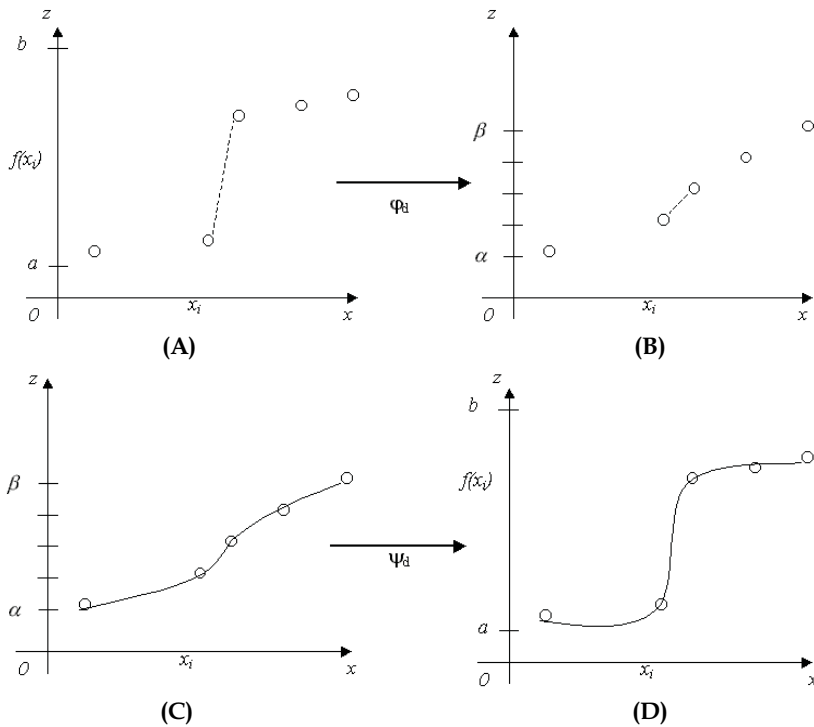


Fig. 2. The preprocessing phase, (A) and (B), transforms the values $f(x_i)$ using a scale transformation φ_d . After preprocessing, B, the local variations in the data have been drastically reduced. Therefore, it is possible to obtain a regular approximant T^d with no significant oscillations using a usual C^1 spline operator (see subsection 2.2), as shown in (C). A second scale transformation ψ_d is subsequently applied to the values of the approximant in a postprocessing phase, (D), to map them back and obtain the final approximant. It is important to mention that the scale transformations used do not create spurious oscillations, as illustrated in (D).

2.1 Scale transformations

In this section, we give a construction of the scale transformation families by generalizing the technique seen in Torrens, 1991. These scale transformations are realistic in the sense that, as classical transformations, they are monotonous.

Preprocessing of the Data: Family φ_d of Scale Transformations

The goal of the scale transformation φ_d is to reduce the variations in the data set. We first construct φ_d , and, in order to study the convergence of the approximation, we then establish the convergence of φ_d to a function φ when the number of data points tends to infinity (i.e., $d \rightarrow 0$): Let $[\alpha, \beta]$ be an interval of \mathbb{R} , and $\{u_i\}_{i=1, \dots, p(d)}$ the following regular subdivision, for $i = 1, \dots, p(d)$:

$$\alpha = u_1 < u_2 < u_3 < \dots < u_{p(d)-1} < u_{p(d)} = \beta \text{ and } u_{i+1} - u_i = \frac{\beta - \alpha}{p(d) - 1} \quad (5)$$

These interval and subdivision are chosen by the user. When dealing with surface approximation from rapidly varying data, we choose the interval to be $[0, 1]$, and an even subdivision of the $\{u_i\}$ that is used to reduce the local variations of the (z_i) . After applying φ_d , we obtain a new data set (x_i, u_i) related to the initial data by $u_i = \varphi_d(z_i)$. When this technique is applied to other problems however, for instance in some applications in imaging when one has an image with homogeneous regions, it can be of interest to increase the variations between pixel values—the (z_i) —; in such a case, Apprato and Gout, 2000 showed that it is possible to choose a nonregular distribution in the interval $[\alpha, \beta]$ to generate variations, and therefore to enhance some features present in the image to facilitate its segmentation.

We introduce $\varphi : [a, b] \rightarrow [\alpha, \beta]$ the C^∞ diffeomorphism that transforms $[a, b]$ into $[\alpha, \beta]$ (such families of transformations are usually called anamorphosis in the geostatistics literature):

$$\varphi(z) = \frac{\beta - \alpha}{b - a}(z - a) + \alpha. \quad (6)$$

We also introduce the function φ_d , for $i=1, \dots, p(d)-1$ and for any $z \in [z_i, z_{i+1}]$,

$$\varphi_d(z) = u_i q_{0m}^0 \left(\frac{z - z_i}{z_{i+1} - z_i} \right) + u_{i+1} q_{0m}^1 \left(\frac{z - z_i}{z_{i+1} - z_i} \right) + \alpha_1(z_i)(z_{i+1} - z_i) q_{1m}^0 \left(\frac{z - z_i}{z_{i+1} - z_i} \right) + \alpha_1(z_{i+1})(z_{i+1} - z_i) q_{1m}^1 \left(\frac{z - z_i}{z_{i+1} - z_i} \right) \quad (7)$$

where the q_{lm}^i , for $i = (0, 1)$, and $l = (0, 1)$, are the basis functions of the finite element of class C^m on $[0, 1]$ (see Ciarlet, 1978) and where, for any $i = 1, \dots, p(d)-1$,

$$\alpha_1(z_i) = \frac{u_{i+1} - u_i}{z_{i+1} - z_i} \text{ and } \alpha_1(z_{p(d)}) = \alpha_1(z_{p(d)-1}). \quad (8)$$

Using relations (5)–(8), we obtain the following results: φ_d implements the interpolation of the (u_i) and φ_d belongs to $C^m([a, b])$:

$$(i) \quad \varphi_d(z_i) = u_i, \text{ for } i=1, \dots, p(d);$$

$$(ii) \quad \varphi_d \in C^m([a, b]).$$

We now consider a *sufficient* convergence hypothesis, which implies that the distribution of the data (z_i) has an asymptotic regularity in the interval $[a; b]$ when d tends to 0, and which is used to establish the convergence of the approximation. This hypothesis is that there exists $C > 0$ and an integer m'' verifying $m'' \geq m \geq 2$ such that, for d small enough; and for any $i = 1, \dots, p(d)-2$, we have

$$\left| 1 - \frac{z_{i+1} - z_i}{z_{i+2} - z_{i+1}} \right| \leq C \left(\frac{b-a}{p(d)-1} \right)^{m''}. \quad (9)$$

We also suppose that the set A^d introduced above is such that there exists $C' > 0$ such that

$$p(d) \leq \frac{C'}{d^2}. \quad (10)$$

Inequation (10), introduced by Arcangéli (1989), expresses a property of asymptotic regularity of the distribution of the data set A^d in $\bar{\Omega}$. Using a compactness argument, Gout, 2002 established that hypotheses (9) and (10) imply that there exists $C'' > 0$, such that $\|\varphi_d\|_{C^m([a,b])} \leq C''$ and

$$\lim_{d \rightarrow 0} \varphi_d = \varphi \text{ in } C^0([a, b]), \quad (11)$$

where φ_d is defined by (7), and φ is defined by (6).

One can notice that the construction of the scale transformations φ_d made in (7) uses a finite difference scheme of order 1 to construct, from the u_i , the first derivatives of φ_d at the points \tilde{z}_i , $i = 1, \dots, p(d)$. Moreover, the option retained in (6), which is to cancel the l derivatives of φ_d at the points \tilde{z}_i for any $l=2, \dots, m$, could be substituted by the option consisting in using a finite difference scheme of order l to define these l derivatives. Let us also mention that we have chosen to construct scale transformations on a finite element basis in order to be able to study the convergence of the approximation.

Postprocessing of the Data: Family ψ_d of Scale Transformations

Similarly to the way we constructed the scale transformations φ_d , we now define a scale transformation family ψ_d that implements the postprocessing of the calculation. We recall that after the preprocessing, the large local variations in the dataset have been drastically reduced; therefore it is possible to approximate the data using a usual spline operator T^d without generating significant oscillations. To map these values back and obtain the approximated values of z , we need to use a postprocessing step, and therefore need to

introduce a family ψ_d , which is almost the inverse of φ_d : as φ_d converges to φ , we construct ψ_d such that ψ_d converges to φ^{-1} . To do so, we define the C^∞ diffeomorphism $\varphi^{-1} : [\alpha, \beta] \rightarrow [a, b]$ inverse of φ defined in Equation (6):

$$\varphi^{-1}(u) = \frac{(u - \alpha)(b - a)}{\beta - \alpha} + a. \tag{12}$$

We also define ψ_d the function, for $i = 1, \dots, p(d) - 1$, and for any $u \in [u_i, u_{i+1}]$,

$$\psi_d(z) = z_i q_{0m}^0 \left(\frac{u - u_i}{u_{i+1} - u_i} \right) + z_{i+1} q_{0m}^1 \left(\frac{u - u_i}{u_{i+1} - u_i} \right) + \beta_1(u_i)(u_{i+1} - u_i) q_{1m}^0 \left(\frac{u - u_i}{u_{i+1} - u_i} \right) + \beta_1(u_{i+1})(u_{i+1} - u_i) q_{1m}^1 \left(\frac{u - u_i}{u_{i+1} - u_i} \right) \tag{13}$$

where the q_{lm}^i , for $i = (0, 1)$, and $l = (0, 1)$, are the basis functions of the finite element of class C^m on $[0; 1]$ (Ciarlet, 1977) and where, for any $i = 1, \dots, p(d) - 1$:

$$\beta_1(u_i) = \frac{z_{i+1} - z_i}{u_{i+1} - u_i} \text{ and } \alpha_1(u_{p(d)}) = \alpha_1(u_{p(d) - 1}). \tag{14}$$

Under hypotheses (9) and (10), Apprato and Gout, 2000 established the following relations:

- (i) $\psi_d(u_i) = z_i, i = 1, \dots, p(d)$;
- (ii) $\psi_d \in C^m([\alpha, \beta])$;
- (iii) there exists $C > 0$; such that $\|\psi_d\|_{C^m([\alpha, \beta])} \leq C$;
- (iv) $\lim_{d \rightarrow 0} \psi_d = \varphi^{-1}$ in $C^0([\alpha, \beta])$.

It is important to mention that (15-i) is one of the key points of the algorithm, that (15-ii) enables us to obtain approximants with high regularity, and that (15-iii) and (15-iv) are used to establish the convergence of the approximation.

2.2 The spline operator

Given a Lagrange dataset $(x_i, (\varphi_d \circ f)(x_i) = \varphi_d(z_i))_{i,d}$ we have to solve the classical problem of constructing an approximant T^d of class C^k (with $k = 1$ or 2 in practice). In this work, we use a smoothing D^m spline, as defined in Arcangéli et al., 2004, which has many advantages: it is possible to implement a local refinement, the matrix of the linear system to solve is banded, and it is possible to study the convergence of the approximation. We have chosen to use a smoothing D^m spline and not an interpolation spline because we want to be able to work with large datasets of up to several hundreds of thousands of points, and in that case, a smoothing spline is far less expensive than an interpolation spline. We consider the functional, for any Φ belonging to $H^m(\Omega)$,

$$J_\varepsilon^d(\Phi) = \left\langle \rho^d(\Phi - \varphi_d \circ f) \right\rangle_{p(d)}^2 + \varepsilon |\Phi|_{m, \Omega}^2 \tag{16}$$

where $\rho^d \in L(H^m(\Omega), IR^{p(d)})$ is defined by $\rho^d f = (f(a))_{a \in A^d} \in IR^{p(d)}$, $|\cdot|_{m,\Omega}$ is the usual semi-norm on $H^m(\Omega)$, $\langle \cdot \rangle_{p(d)}$ is the Euclidean norm in $\mathbb{R}^{p(d)}$, and ε a smoothing parameter. We call σ_ε^d the D^m -smoothing spline on Ω relative to $\varphi_d \circ f$ which is the unique solution of the minimization problem: find $\sigma_\varepsilon^d \in H^m(\Omega)$ such that for any Φ belonging to $H^m(\Omega)$:

$$J_\varepsilon^d(\sigma_\varepsilon^d) \leq J_\varepsilon^d(\Phi). \quad (17)$$

The solution σ_ε^d to this problem is also the unique solution of the variational problem: find $\sigma_\varepsilon^d \in H^m(\Omega)$ such that for any Φ belonging to $H^m(\Omega)$:

$$\langle \rho^d \sigma_\varepsilon^d, \rho^d \Phi \rangle_{p(d)} + \varepsilon \langle \sigma_\varepsilon^d, \Phi \rangle_{m,\Omega} = \langle \rho^d(\varphi_d \circ f), \rho^d \Phi \rangle_{p(d)}. \quad (18)$$

Uniqueness of the solution can be proved using the Lax-Milgram lemma and results by Necas, 1967 to establish an equivalence of norms.

In order to compute σ_ε^d , we choose to discretize it on a finite element basis, which enables us to obtain a small sparse linear system. We choose the generic Bogner-Fox-Schmit (BFS) rectangular finite element (see Ciarlet, 1977). In what follows, we use either the BFS of class C^0 or of class C^1 in order to obtain a C^0 or C^1 approximant. In the following, we write σ_ε^d instead of T^d .

2.3 Convergence results

We first give the convergence of the D^m spline operator σ_ε^d related to the transformed data $(\varphi_d \circ f)$ to the function $(\varphi \circ f)$ when d tends to 0. We obtain this result using the convergence of φ_d to φ , using the fact that Apprato et al., 1987, showed that, for any function g , we have $\lim_{d \rightarrow 0} \sigma_\varepsilon^d(g) = g$.

Keeping the notation of the previous sections, and since $(\varphi_d \circ f)$ is bounded in $C^m(\overline{\Omega})$, Apprato and Gout, 2000, proved that

$$\lim_{d \rightarrow 0} \sigma_\varepsilon^d(\varphi_d \circ f) = \varphi \circ f \text{ in } C^0(\overline{\Omega}). \quad (19)$$

From this result, using a compactness argument, Apprato and Gout, 2000 established a theoretical result concerning the convergence of the approximation:

$$\lim_{d \rightarrow 0} (\psi_d \circ \sigma_\varepsilon^d(\varphi_d \circ f)) = \varphi^{-1} \circ \varphi \circ f = f \text{ in } H^{m-\Theta}(\Omega), \quad (20)$$

for any $\Theta > 0$ such that $\Theta < m - 1$ (\Rightarrow continuous embedding of $H^{m-\Theta}(\Omega)$ into $C^0(\overline{\Omega})$). Note that if we take $n = 2$ and $m = 3$, the convergence takes place in $H^{2-\Theta}(\Omega)$ for any $\Theta \in]0,1[$.

2.4 Numerical examples

The Piton de la Fournaise is a volcano located in the Indian Ocean, in the Réunion Island, France. This volcano exhibits strong topographic variations near its summit, due to the presence of a caldera and of two steep river valleys in its southwestern part, as can be seen on the picture of the volcano presented in Figure 3. The maximum height of the volcano is 2.6 km, and the depth of the valleys reaches more than 1000 m in several places. Being able to describe the topography of such regions exhibiting rapid local variations with at least C^0 regularity, or even C^1 regularity, is important in many fields in geophysics. For example, this description of the topography can be an input to numerical modeling codes that study the propagation of pyroclastic flows or lava flows, and related hazards; other examples are seismic site effects and ground motion amplification due to topographic features. In both cases, to avoid creating numerical artefacts, it is important not to introduce spurious oscillations in the description of the model itself. Otherwise, it is well known that in the context of curvilinear spectral element modeling of elastic wave propagation, artificial diffraction points appear at the edges between elements, which significantly affects the behavior of surface waves. To demonstrate the efficiency of our method, we create C^0 and C^1 approximants from a set of 8208 data points taken from a DEM of the summit. The data points in the DEM have been obtained by digitizing a map of the area. In this DEM, the height is given on an evenly spaced grid of 76×108 points, with a grid spacing of 200 m. Therefore the considered region has a dimension of 15 km in the East–West direction, and 21.4 km in the North–South direction. This DEM is shown in Figure 4 using a top view with isocontours representing the height of the topography every 0.2 km.

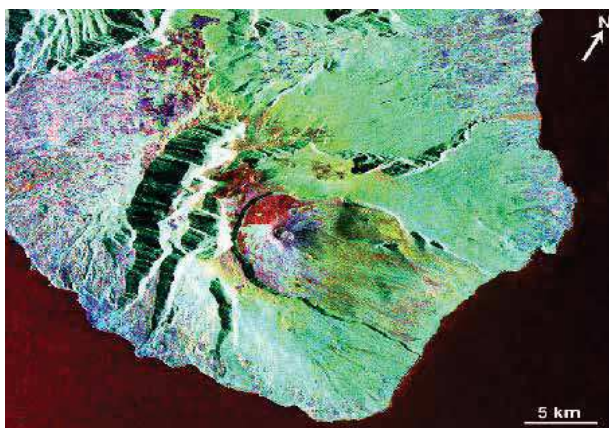


Fig. 3. Image of the Piton de la Fournaise volcano in the Réunion Island, Indian Ocean, France. One can clearly see the summital caldera, and the two steep valleys in the South–West. The size of the region represented is approximately 40×35 km. The height of the volcano is 2.6 km. Image taken as part of the Space Shuttle SIR-C/X-SAR radar missions, courtesy of Pete Mouginis-Mark, University of Hawaii.

In the preprocessing step, we choose a regular distribution of the u_i in $[\alpha, \beta] = [0, 1]$ in order to reduce the large variations in the data set. The approximants are subsequently obtained by discretizing the D^m spline in a finite-element space. In the case of the C^0 approximant, we use 30×40 rectangular C^0 BFS finite elements, each having four degrees of freedom. In the case of the C^1 approximant, we use 15×20 rectangular C^1 -BFS finite elements, each having sixteen degrees of freedom. In both cases, the smoothing parameter ε is taken to be 10^{-6} .

In Figure 4, we show a three-dimensional representation of the C^1 approximant after postprocessing, evaluated on an evenly spaced grid comprising 200×200 points. The grid spacing in the East-West direction is therefore 107.54 m, and the one in the North-South direction is 75.37 m. From the figure it is clear that the results do not exhibit strong oscillations, even though the use of such a dense grid for the evaluation of the approximant is expected to enhance the artefacts generated by the approximation method. To compare this approximant to the original dataset more precisely, in Figure 5 we present a top view of the approximated values, with isocontours representing the height every 0.2 km, in addition to the same plot for the original dataset. It is clear from these plots that the approximant is very close to the original data, with local variations smoothed as expected. One can notice that the approximant does not exhibit significant oscillations even in the difficult regions of the model, particularly the two valleys. To demonstrate this more quantitatively, we evaluate the quadratic error for the two approximants. In the case of the C^0 approximant, we find that the error is 4.96×10^{-4} ; in the case of the C^1 approximant it is 4.01×10^{-4} . Such values are considered as very good ones in the context of surface approximation, and show the efficiency of the proposed approach for this case with rapidly varying data. In the entire dataset, the maximum error measured is 5.5%, corresponding to an absolute error of 56 m. This maximum error occurs in a region located on the edge of the steep valleys, where the local variations are the strongest, as expected. More detailed studies of the approximation error, and evidence that the rate of convergence is higher in this method than in usual approaches with no preprocessing, such as thin plate spline or splines under tension can be found in Schoenberg, 1960.

We have presented a new method to fit rapidly varying geophysical data. The ability to suppress, or at least significantly reduce, oscillations of the surface near steep gradients has been demonstrated. The scale transformation families introduced provide more control on the behavior of the approximant, without any particular *a priori* knowledge of the location of the large variations in the dataset. The regularity obtained, which can be C^0 , C^1 , or higher, enables us to describe the topography of real geophysical surfaces accurately. We have shown the good properties of this approach by applying it to the real case of the Piton de la Fournaise volcano.

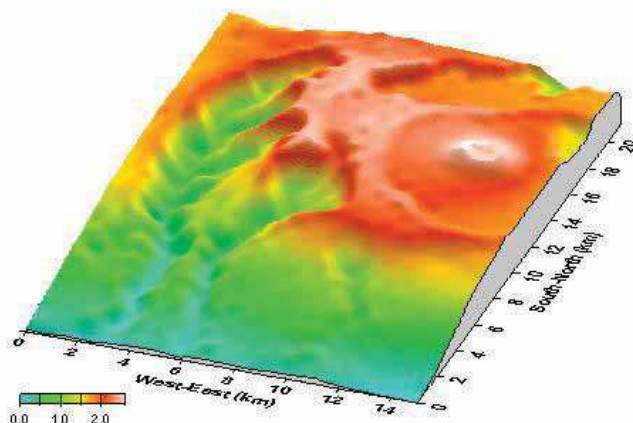


Fig. 4. Three-dimensional view of the C^1 approximant, after post-processing, obtained for the Piton de la Fournaise volcano from the Digital Elevation Model. The scale represents the height of the topography, from 0 to 2.6 km. The image has been generated with no vertical exaggeration. The approximant has been evaluated on an evenly spaced grid comprising 200×200 points. No significant oscillations can be observed, even in the difficult regions of the model, which are mainly the two valleys, and also the caldera. In this example, we have discretized the spline using 15×20 BFS finite elements, each having sixteen degrees of freedom.

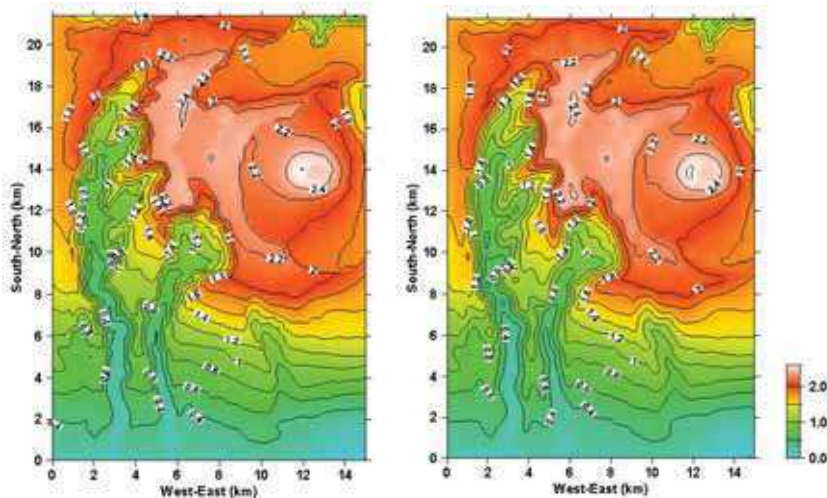


Fig. 5. Comparison between the isocontours obtained from the original dataset of the DEM. Left : Isocontours of the DEM of the Piton de la Fournaise volcano. The DEM is given on a grid of 76×108 points, with a uniform grid spacing of 200 m. The height of the summit is 2.6 km. One can clearly observe the slopes of the two steep valleys, and the isocontours of the C^1 approximant after postprocessing (right), as in the three-dimensional view of Figure 4.

The general agreement is excellent, and it is important to notice that no significant oscillations can be observed, even in the two steep valleys. Isocontours represent the height of the topography every 0.2 km. The gray scale also indicates the height of the topography, from 0 to 2.6 km.

3. Seafloor surface approximation from bathymetric dataset

3.1 Modelling

The problem of surface approximation from a given set of curves can be formulated as follows: from a finite set of curves $F_j, j = 1, \dots, N$ (the bathymetry ship track curves in our case) in the closure of a bounded nonempty open set $\Omega \subset \mathbb{R}^2$, and from a function f defined on $F = \bigcup_{j=1, \dots, N} F_j$, construct a regular function Φ on Ω approximating f on F , i.e.:

$$\Phi|_F \cong f|_F. \quad (21)$$

We can assume that Ω is a connected set, with a Lipschitz-continuous boundary (following the definition of Necas, 1967), that for any integer j , with $j=1, \dots, N$, F_j is a nonempty connected subset in F , and that, for simplicity, f is the restriction on F of a function, still denoted by f , that belongs to the usual Sobolev space $H^m(\Omega)$, with the integer $m > 1$. We also assume that the approximant Φ belongs to $H^m(\Omega) \cap C^k(\bar{\Omega})$ with $k = 1$ or 2 , where $\bar{\bullet}$ denotes the closure. The main interest of such a regularity for Φ is that it allows one to obtain a final surface that can later be used directly as an input model in a different application, such as ray tracing, image synthesis, or numerical simulation.

Let us define, for any v belonging to $H^m(\Omega)$, $\rho v = v|_F$ where ρ is a linear operator and let us introduce the convex set $K = \{v \in H^m(\Omega), \rho v = \rho f\}$. Then we consider the minimization problem of finding $\sigma \in K$ such that for any $v \in K$:

$$|\sigma|_{m,\Omega} \leq |v|_{m,\Omega}, \quad (22)$$

where $|\bullet|_{m,\Omega}$ is the usual semi-norm on $H^m(\Omega)$. If $L^2(F)$ is equipped with the usual norm

$$\|v\|_{0,F} = \left(\sum_{j=1}^N \int_{F_j} v^2 ds \right)^{1/2}, \quad (23)$$

and under the hypothesis that for any $p \in P_{m-1}(\bar{F})$, $p|_F = 0 \Rightarrow p \equiv 0$, we know, based upon a compactness argument (Necas, 1967), that the function $\|\bullet\|$ defined by

$$\|u\| = \left(\|\rho u\|_{0,\Omega}^2 + |u|_{m,\Omega}^2 \right)^{1/2} \quad (24)$$

is a norm on $H^m(\Omega)$ which is equivalent to the usual norm $\|\bullet\|_{m,\Omega}$ on $H^m(\Omega)$. Then the solution σ of the interpolation problem (22) is the unique element of minimal norm $\|\bullet\|$ in K that is convex, nonempty, and closed in $H^m(\Omega)$. Hence we could take the solution $\Phi = \sigma$ when $m > k + 1$. Unfortunately, it is often impossible to compute σ using a discretization of problem (22), because in a finite dimensional space, it is generally not possible to satisfy an infinity of interpolation conditions. Therefore, to take into account the continuous aspect of the data on F , we instead choose to define the approximant Φ as a fitting surface on the set:

$$\left\{ (x_1, x_2, x_3) \in \mathbb{R}^3, x_3 = f(x_1, x_2), (x_1, x_2) \in F_j, j = 1, \dots, N \right\}. \quad (25)$$

In this work, we propose to construct a variant of the “smoothing D^m -spline,” seen in previous sections, that will be discretized in a suitable piecewise-polynomial space. The use of such spline functions has been shown to be efficient in the context of geophysical applications such as Ground Penetrating Radar data analysis (Apprato et al., 2000) or the creation of Digital Elevation Models describing topography (Gout and Komatitsch, 2000). Let us present in this section the theoretical aspects of the method. We first introduce a functional J_ε that we shall minimize, defined on $H^m(F)$ by

$$J_\varepsilon(v) = \|v - f\|_{0,F}^2 + \varepsilon |v|_{m,\Omega}^2, \quad (26)$$

where $\varepsilon |v|_{m,\Omega}^2$ is a smoothing term, $\varepsilon > 0$ being a classical smoothing parameter. The key idea

here is that the fidelity criterion to the data $\|v - f\|_{0,F}^2$ honors their continuous aspect. We

now need to numerically estimate this L^2 -norm, which is done using a quadrature formula. In this respect, the approach is quite different from more classical techniques that usually simply make use of a large number of data points on F in order to solve the approximation problem. For any integer $j, j = 1, \dots, N$, and any $\eta > 0$, let $\{\zeta_i\}_{1 \leq i \leq L}$ be a set of $L = L(j)$ distinct

points $\zeta_i = \zeta_i(j) \in \overline{F_j}$ such that $\max_{1 \leq i \leq L-1} \delta(\zeta_i, \zeta_{i+1}) \leq \eta$, where δ is the Euclidean distance in

\mathbb{R}^2 . This relation implies that the distance between two consecutive ζ_i is bounded by η , it

also enables one to study the convergence of the approximation when η tends to 0. The $\{\zeta_i\}$

will also be the nodes of a numerical integration formula. Let us also introduce a set $(\lambda_i)_{1 \leq i \leq L}$ of real numbers (that will be the weights of a quadrature formula) such that

$\lambda_i = \lambda_i(j) > 0$, and let us define, for any $v \in C^0(\overline{F_j}), \forall \eta > 0$,

$$l_j^\eta(v) = \sum_{i=1}^L \lambda_i v(\zeta_i), \quad (27)$$

and for any $v \in C^0(\overline{F_j})$,

$$l(v) = \sum_{j=1}^N l_j^\eta(v). \quad (28)$$

In what follows, we will suppose that, for any $v \in H^m(\overline{F})$ and any $\eta > 0$, there exists $C > 0$ such that

$$\left| l_j^\eta(v^2) - \|v\|_{0,F_j}^2 \right| \leq C\eta \|v\|_{m,\Omega}^2. \quad (29)$$

When this hypothesis is satisfied, one can consider l as a theoretical quadrature formula for $\|v\|_{0,F_j}^2$. Note that in some case ($N=1$), $l(v)$ is a quadrature formula for the curvilinear

integral $\int_F v ds$. Note also that in most applications the F_j are polygonal curves, and one can,

therefore, use a classical quadrature formula (e.g., Arcangéli and Gout, 1976, or Gout and Guessab, 2001).

For the discretization, we proceed like in Section 2, using a finite element space.

3.2 Application to surface reconstruction from bathymetry ship track data in the Marianas trench

Detailed bathymetry maps are essential in several fields in geophysics, such as oceanography and marine geophysics. Historically, over the past decades, research vessels have collected a large number of depth echo soundings, also called SONAR (for "SONic Navigation And Ranging") bathymetry ship track data. Many of these measurements have been compiled to produce global bathymetry maps (e.g., Canadian Hydrographic Office in 1981). In recent years tremendous advances in satellite altimetry have enabled researchers to produce very detailed bathymetry maps independently of satellite gravity field measurements. However, long-wavelength variations of the depth of the ocean floor are difficult to constrain using satellite altimetry, and ship track data are still often used instead for that purpose. It is, therefore, of interest to address the issue of producing a bathymetry map from a given set of SONAR bathymetry ship tracks. Let us mention that SONAR ship tracks are typically acquired as a discrete set of measurement points, as opposed to continuous recording. However, the typical horizontal interval between measurement points is always small compared to expected bathymetry variations; therefore, in the context of this study the dataset can be considered as consisting of smooth continuous lines.

As presented in Url, 2009, in order to understand the shape of the seafloor, oceanographers go out on ships and collect sonar data. Sonar data are collected using echosounders and side-scan sonar systems. The digital data are then converted into maps and images.

How does this work?

Echosounders : Since World War II echosounders have been used to determine water depths of the oceans. Echosounders are usually attached to the hull of a ship. The echosounder sends an outgoing sound pulse into the water. The sound energy travels through the water to the ocean bottom where it is reflected back towards the source, received, and recorded.

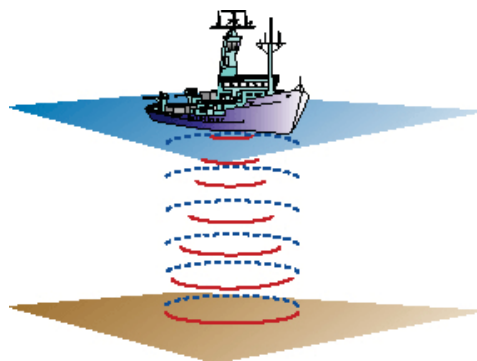


Fig. 6. Sound travels from the ship to the seafloor and is reflected back. The time it takes is converted into distance yielding water depth. (Credit : www.womenoceanographers.org)

The time that it takes for the sound to make the round trip to the seafloor is accurately measured. Water depth is determined from the travel time and the speed of sound in water. Water depth can be estimated simply by using an average sound speed and the following relationship: $\text{Distance} = \text{speed} \times \text{time}/2$, (the time is divided by 2 to take into account the round trip from the echosounder to the seafloor). The unique drawback of such an echosounder is that it will only give one depth at each time. That is why multibeam echosounders have been created...

How are water depths turned into a map?: As a ship steams ahead through the water, multibeam echosounders provide water depths for a swath of the seafloor. The water depths are located in space using satellite navigation. From these data, oceanographers can make maps of the seafloor that resemble topographic maps of land areas. In the early times, bathymetry maps were drawn by hand. Contours (lines) of equal water depth were drawn through a grid of numbers that had been plotted on a sheet of paper. Colors, put on by hand, indicated regions of equivalent water depth. Eventually computers took over and produced paper charts of the data, contoured and automatically colored. Now computer softwares enable individual scientists to process the data and display them on their own computer monitors. Maps can be imported into graphic software applications and annotations and other marks can be added.

"Side-scan" sonars: Similar to the multibeam echosounder, the sound transmitted by a side scan sonar instrument travels to the seafloor, bounces off the seafloor, returns to the instrument, and is recorded. In the case of a side-scan sonar, it is the intensity or strength of the returning acoustic signal that is recorded. This is controlled primarily by the slope of the seafloor and by what the seafloor is made of. A stronger return is received if the seafloor slopes down to the instrument. Also, the return is stronger if the seafloor is made of bare rocks. The strength of the return is much lower if the seafloor is covered by mud or sand. Volcanoes and other features that stick up above the surrounding seafloor will cast acoustic

shadows. These shadows are just like the shadow behind a person when a flashlight is shone on him.

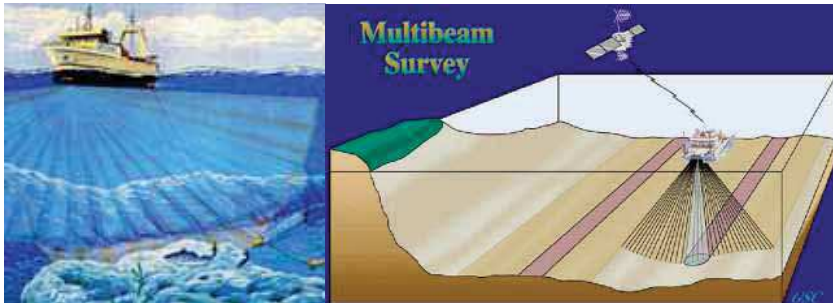


Fig. 7. Cartoon from a NOAA web site showing the swath of seafloor insonified by the multibeam echosounder. (Credit : NOAA and GSC)

Converting intensity into an image: The strength of the sound recorded by the side-scan sonar instrument is converted into shades of gray. A very strong return, say from bare rock, is white; a very weak return is black. The echo strengths that fall between these two extremes are converted into different shades of gray. Historically, side scan sonar data have been displayed on a hard copy paper recorder. The paper chart used to be the most convenient method for displaying and storing these data (as well as bathymetry data). Since the 1980s or so, software and hardware have been developed to process side scan data using computers and display the data on computer screens.

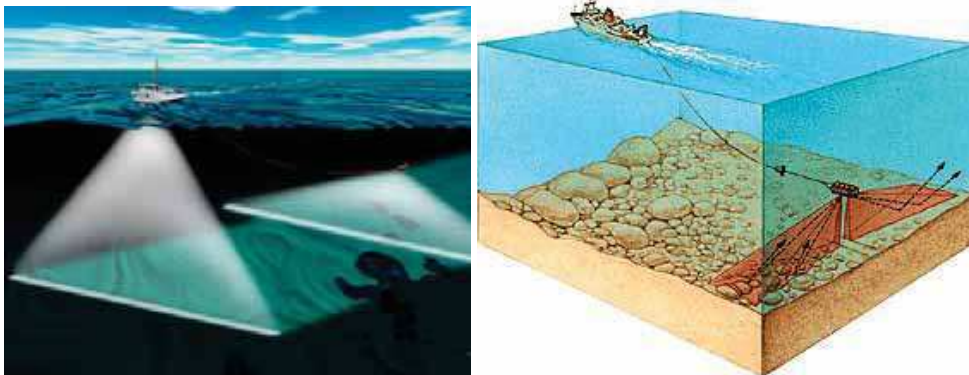


Fig. 8. Left : Hull-mounted multibeam sonar (left) and towed side scan sonar (right). NOAA – Right : The side scan sonar instrument is towed by the ship. Sound is transmitted into the water and images are made based on the strength of the recorded return. (credit : NOAA)

We select the region of the Marianas trench (Figure 9). The trench is located in the North Pacific ocean, east of the South Honshu ridge, parallel to the Mariana Islands. It corresponds to the subduction zone where the fast-moving Pacific plate converges against the slower moving Philippine plate. It is also the place on Earth where the oceans are the deepest, reaching a maximum depth of slightly more than 11 km in the so-called “Challenger Deep”

area (Figure 9). This region is ideal to test our surface approximation technique because it has been thoroughly studied; therefore, many ship track datasets are available. We select a 45×45 km area, corresponding to latitudes between 11.2^\pm and 11.6^\pm North, and longitudes between 142^\pm and 142.4^\pm East. We use 16 tracks from the database assembled by **David T. Sandwell** and coworkers at the University of California, San Diego (<http://topex.ucsd.edu>). Each individual track contains between 62 and 152 points giving depth for a given latitude and longitude. The total number of points in the whole dataset is 1576. The depth varies between 6779 and 10952 m. As can be seen on Figure 9, the ship track coverage of the area is nonuniform. Note in particular the lack of data in the north-east and south-east corners. Fortunately, data coverage is much better near the center in the deepest part of the trench. We create an approximant using 169 quadrangular Bogner-Fox-Schmit finite elements defined on a regular 13×13 grid in the horizontal plane in the area under study. As underlined in the previous section, these elements enable us to obtain an approximant with C^1 regularity. Figure 9 shows a 3D view of the final surface obtained, as well as the original set of ship tracks. For display purposes, the approximant has been evaluated on a regular 200×200 grid of points and a vertical exaggeration factor of 3 has been applied. By comparing with Figure 9 and with the ship tracks, one can see that the smooth surface obtained correctly reproduces the general characteristics of the bathymetry of the region, and behaves satisfactorily even in the areas where the data coverage is sparse.

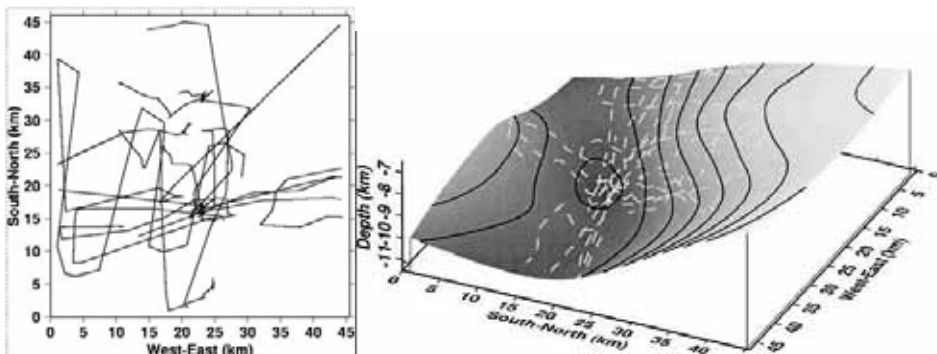


Fig. 9. **LEFT** : We focus on a 45×45 km region in the south-west of the Marianas trench. We use 16 bathymetry ship tracks, each containing between 62 and 152 points. The entire set of curves contains 1567 points. Each point gives depth for a given latitude and longitude. On this top view the coordinates have been mapped using the Universal Transverse Mercator (UTM) projection. The depth in the dataset varies between 6779 and 10952 m. One can see that the ship track coverage is nonuniform. For instance we have little information in the north-east and south-east corners of the area. **RIGHT** : We construct a bathymetry map from the set of 16 ship track data curves using a regular grid of 13×13 quadrangular Bogner-Fox-Schmit finite elements of class C^1 . For display purposes, the approximant obtained has been evaluated on a regular 200×200 grid of points, and a vertical exaggeration factor of 3 has been applied. The original 16 ship tracks are also shown (dashed lines) to illustrate the quality of the obtained surface. The isolines represent bathymetry every 500 m. By comparing with Figure 9 (right), one can see that we are correctly reproducing the general trends of the bathymetry of the area.

Thank You for previewing this eBook

You can read the full version of this eBook in different formats:

- HTML (Free /Available to everyone)
- PDF / TXT (Available to V.I.P. members. Free Standard members can access up to 5 PDF/TXT eBooks per month each month)
- Epub & Mobipocket (Exclusive to V.I.P. members)

To download this full book, simply select the format you desire below

